Vol.2, No.2, Page 197- 204, 2024 https://doi.org/10.59628/jast.v2i2.899 ISSN 2958-9568 JAST

SUN PUBLISHER

مجلة جامعة صنعاء للعلوم التطبيقية والتكنولوجيا

Sana'a University Journal of Applied Sciences and Technology

https://journals.su.edu.ye/index.php/jast/

Intensity distribution of the partially coherent Gaussian Schell vortex beam diffracted by classical axicon

Shukri A. M. Kaid[1,2] *, Hatim O. Al-Nadary[1,3]*, Mohammad S. Qusailah [1], Hassan AL-Ahsab [4] and Abdu A. Alkelly [1]

[1]**Department of Physics, Faculty of Science, University of Sana'a, Sana'a, Yemen,**
[2]**Physics Department, Faculty of Science, Taiz University, Taiz, Yemen,**
[3]**Physics Department, College of Science and Arts, Najran University, Najran, Saudi Arabia,**
[4]**Physics Department, Faculty of Applied Science, Thamar University, Thamar, Yemen.**

*Corresponding author: shukekaid530@gmail.com
*Corresponding author: hoalnadary@nu.edu.sa

Abstract

Based on the mathematical framework of the partially coherent Gaussian Schell model vortex (PCGSMV) beam and the Huygens-Fresnel integral, we conducted a study to analyze the intensity distribution and depth of focus (DOF) of the PCGSMV beam as it propagates through a classical axicon. Our numerical results indicate the influence of factors such as the beam width, spatial degree of coherence, topological charge, and axicon base angle on the intensity distribution and DOF. In addition, we investigated the relationship between the beam spot size and propagation distance, as well as the effects of the spatial degree of coherence and propagation distance on the intensity profile. Our findings highlight the importance of the intensity values along the DOF for various applications, including the optical trapping and manipulation of micro-particles.

Article Info

Keywords:
Gaussian Schell model, vortex beam, Huygens-Fresnel integral, depth of focus, classical axicon

Article History:
Received: 27-February-2024,
Revised: 27-March-2024,
Accepted: 6-April-2024,
Available online: 5 May 2024

1. INTRODUCTION

Axicons are versatile optical devices that produce focal lines instead of focal point generated by lenses [1]. Axicons have attracted increasing attention because of their diversity and utility in generating various significant beam shapes within the focal region [1–4]. The classical axicon, characterized by an on-axis intensity linearly increasing along the optical axis, has been employed for the creation of non-diffracting Bessel beams [5], as well as for producing diverse focal shapes, such as hollow laser beams [6], double focal spots [4], thin-sheet lights [7], tight focal spot sizes [2], flat-topped beams [8], and three-dimensional dark spots [9]. As a result, the linear axicon has been recognized as a crucial optical component in long-range alignment [10], laser machining [11], Bose–Einstein condensates [12], and particle manipulation [13]. Recently, partially coherent (PC) beams have demonstrated distinctive properties and have proven their superiority in a broad range of applications including optical communication [14], noise reduction in photography [15], laser nuclear fusion [16], and classical ghost interference [17]. The Gaussian Schell model (GSM) beams are typical types of PC beams that have distinctive features, encompassing transverse intensity and degree of coherence, making them highly applicable in diverse areas, including optical communication and ghost imaging [18]. Alkelly et al. conducted a study on the intensity distribution and focal depth of an axicon under illumination using a Gaussian Schell-model beam [19]. Partially coherent GSM beams have undergone thorough theoretical and experimental investigations, and their simple functional expressions make them applicable to different contexts such as free-space optical communication [14], optical scattering [20], and particle trapping [21]. Recent studies

have focused on the unique attributes of vortex beams, which are characterized by spiral wavefront structures and ring shapes. These features have led to the broad recognition of vortex beams for their various applications in focal shaping, particle manipulation, optical patterning, optical tweezers, non-linear optics, and laser communications [22–24]. Partially coherent vortex (PCV) beams have attracted considerable interest owing to their concealed correlation singularities and distinctive propagation properties, encompassing aspects such as beam shaping and self-reconstruction [25, 26]. Moreover, the Partially coherent GSM vortex beam represents a typical type of vortex beam extensively studied in various media, including gradient index media, turbulent plasma, atmosphere, free space, oceanic environments, and biological tissues [27–35]. Lian-zhou et al. studied the properties of a PCV beam focused by an aperture lens [36]. To the best of our knowledge, PCGSMV beam propagation through an axicon has not been explored. This study specifically focuses on analyzing the intensity distribution of a PCGSMV beam diffracted by a classical axicon. In additional, it aims to investigate the impact of the axicon's base angle, topological charge, waist width of the PCGSMV beam, and spatial correlation length on both the intensity and depth of focus. Using the extended Huygens-Fresnel integral and employing the stationary phase approach, we developed a general formula to describe the intensity distribution of a PCGSMV beam diffracted by a classical axicon.

2. THEORETICAL FORMULATION

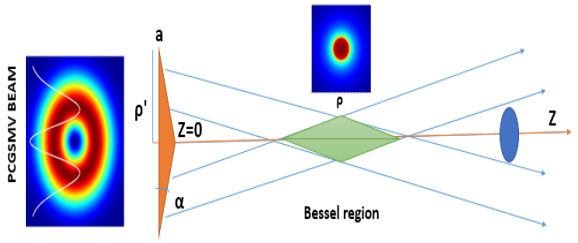

Figure 1. Schematic diagram for beam ray (PCGSMV).

Figure (1) is a schematic diagram represents the beam transfer through a system consists of lens and axicon (lensacon). In this framework, the initial field of the Gaussian vortex (GV) beam at plane $z = 0$ in cylindrical coordinates can be written as [25, 36]

$$u(\boldsymbol{\rho}', z = 0) = \sqrt{G_0}\, \exp\left[i\, m\, \phi'\right] \exp\left[-\frac{\rho'^2}{w^2}\right], \quad (1)$$

where, G_0 is a real constant characterizing the field amplitude of the Gaussian beam, $\rho' = \sqrt{x^2 + y^2}$, w is the waist width of the Gaussian beam, ϕ' is the azimuthal angle, and m is the topological charge. When $m = 0$, Eq. (1) is reduced to a Gaussian beam. The cross-spectral density (CSD) of the PCGSMV beam, considering the Schell-correlator at the source plane, is defined as [25]

$$W_{in}(\rho_1', \rho_2', z = 0) = \left\langle u^*(\rho_1', z = 0) u(\rho_2', z = 0) \right\rangle, \quad (2)$$

where $\boldsymbol{\rho}_1'$ and $\boldsymbol{\rho}_2'$ are two arbitrary points on the source plane. By considering the correlation function, which is expressed as $\eta(\rho_1' - \rho_2') = \exp\left[-\frac{|\rho_1' - \rho_2'|^2}{2\sigma^2}\right]$, where $\boldsymbol{\rho}_1' = (\rho_1', \phi_1')$ and σ are the spatial correlations of coherence length. We can rewrite Eq. (2) as [36, 37]

$$\begin{aligned} W_{in}(\rho_1', \rho_2', z = 0) =& G_0 \exp\left[i\, m\, (\phi_2' - \phi_1')\right] \\ & \times \exp\left[-({\rho_1'}^2 + {\rho_2'}^2)\left(\frac{1}{w^2} + \frac{1}{2\sigma^2}\right)\right] \\ & \times \exp\left[\frac{\rho_1' \rho_2' \cos(\phi_2' - \phi_1')}{\sigma^2}\right]. \end{aligned} \quad (3)$$

The diffracted field of the PCGSMV beam $u(\rho, z)$ at z distance from the classical axicon in the Huygens-Fresnel (H-F) integral approach is expressed as [19, 38]

$$\begin{aligned} u(\rho, z) =& \sqrt{G_0}\, \left(\frac{-i\ k}{2\, \pi\, z}\right) \exp\left[i\, k\, z\right] \\ & \times \int_0^a \int_0^{2\pi} A(\rho')\, \exp\left[\frac{i\, k}{2\, z}\, |\rho - \rho'|^2\right] \rho' d\rho' d\phi', \end{aligned} \quad (4)$$

where where $k = \frac{2\pi}{\lambda}$, λ is the wavelength of the beam and $A(\rho')$ is defined as

$$A(\rho') = u(\rho', z = 0) A_{axicon}(\rho'), \quad (5)$$

where $A_{axicon}(\rho')$ is the axicon transmission function, that is given as [1, 39]

$$A_{axicon}(\rho') = \exp\left[-i\, k\, \rho' (n - 1)\, \alpha\right], \quad (6)$$

where α refers to the axicon base angle and n represents the refractive index of the axicon. The field diffraction can be computed from the axicon plane with cylindrical coordinates $(\rho_1', \phi_1', z = 0)$ to the image plane with cylindrical coordinates (ρ_1, ϕ_1, z) as

$$\begin{aligned} u(\rho_1, \phi_1, z) =& \left(\frac{-i\, k}{2\, \pi\, z}\right) \sqrt{G_0}\, \exp\left[i\, k\, \left(z + \frac{{\rho_1}^2}{2z}\right)\right] \\ & \times \int_0^a \int_0^{2\pi} \rho_1' \exp\left[i\, m\, \phi_1'\right] \exp\left[-\frac{{\rho_1'}^2}{w^2}\right] \\ & \times \exp\left[\frac{i\, k\, {\rho_1'}^2}{2z}\right] \exp\left[-i\, k\, \rho_1'\, ((n - 1)\, \alpha)\right] \\ & \times \exp\left[\frac{-i\, k\, \rho_1\, \rho_1' \cos(\phi_1 - \phi_1')}{z}\right] d\rho_1' d\phi_1'. \end{aligned} \quad (7)$$

The CSD of the PCGSMV beam propagating through classical axicon described by formula

$$W_{out}(\rho_1, \rho_2, \phi_1, \phi_2, z) = \left\langle u^*(\rho_1, \phi_1, z) * u(\rho_2, \phi_2, z) \right\rangle. \quad (8)$$

Substituting Eq. (7) into Eq. (8), and putting $\rho_1 = \rho_2 = \rho$

and $\phi_1 = \phi_2 = \phi$, Eq. (8) can be written as

$$W_{out}(\rho,\phi,z) = \left(\frac{k}{2\pi z}\right)^2 G_0 \int_0^a \int_0^a \int_0^{2\pi} \int_0^{2\pi} (\rho_1'\rho_2') \times \exp\left[i\,k\,(\rho_1' - \rho_2')\,((n-1)\,\alpha)\right] \times \exp\left[-(\rho_1'^2 + \rho_2'^2)\left(\frac{1}{w^2} + \frac{1}{2\sigma^2}\right)\right] \times \exp\left[\frac{\rho_1'\,\rho_2'\,\cos(\phi_1' - \phi_2')}{\sigma^2}\right] \exp\left[\frac{-i\,k\,\left(\rho_1'^2 - \rho_2'^2\right)}{2z}\right] \times \exp\left[\frac{-i\,k\,\rho\,\rho_2'\cos(\phi - \phi_2')}{z}\right] \exp\left[-i\,m\,(\phi_1' - \phi_2')\right] \times \exp\left[\frac{i\,k\,\rho\,\rho_1'\cos(\phi - \phi_1')}{z}\right] d\rho_1'\,d\rho_2'\,d\phi_1'\,d\phi_2'. \tag{9}$$

Using the Jacobi-Anger expansion that is given by [36]

$$\exp\left[\frac{i\,k\,\rho_1\,\rho_1'\cos(\phi - \phi_1')}{z}\right] = \sum_{l=-\infty}^{\infty} (i)^l J_l\left[\frac{k\,\rho_1'\,\rho_1}{z}\right] \times \exp\left[i\,l\,(\phi - \phi_1')\right], \tag{10}$$

where J_l indicates l^{th}-order Bessel function of the first type. Substituting Eq. (10) into Eq. (9), we rewrite Eq. (9) as

$$W_{out}(\rho,z) = \left(\frac{k}{2\pi\,z}\right)^2 G_0 \sum_{l=-\infty}^{\infty} \int_0^a \int_0^a \int_0^{2\pi} \int_0^{2\pi} (\rho_1'\rho_2') \times \exp\left[i\,k\,(\rho_1' - \rho_2')((n-1)\,\alpha)\right] J_l\left[\frac{k\,\rho\,\rho_1'}{z}\right] \times \exp\left[-(\rho_1'^2 + \rho_2'^2)\left(\frac{1}{w^2} + \frac{1}{2\sigma^2}\right)\right] J_l\left[\frac{k\,\rho\,\rho_2'}{z}\right] \times \exp\left[\frac{-i\,k\,\left(\rho_1'^2 - \rho_2'^2\right)}{2z}\right] \exp\left[\frac{\rho_1'\,\rho_2'\cos(\phi_2' - \phi_1')}{\sigma^2}\right] \times \exp\left[i\,(l+m)(\phi_2' - \phi_1')\right] d\rho_1' d\rho_2' d\phi_1' d\phi_2'. \tag{11}$$

Using the relation [36]

$$\int_0^{2\pi} \int_0^{2\pi} \exp\left[\frac{\rho_1'\,\rho_2'\cos(\phi_2' - \phi_1')}{\sigma^2}\right] \times \exp\left[i\,(m+l)(\phi_2' - \phi_1')\right] d\phi_1' d\phi_2' = 4\pi^2 I_{(m+l)}\left[\frac{\rho_1'\,\rho_2'}{\sigma^2}\right], \tag{12}$$

and substituting Eq. (12) into Eq. (11), we can rewrite Eq. (11) as

$$W_{out}(\rho,z) = \left(\frac{k}{z}\right)^2 G_0 \sum_{l=-\infty}^{\infty} \int_0^a \int_0^a (\rho_1'\rho_2') \times \exp\left[i\,k\,((n-1)\,\alpha)\,(\rho_1' - \rho_2')\right] J_l\left[\frac{k\,\rho\,\rho_2'}{z}\right] \times \exp\left[\frac{-i\,k\,\left(\rho_1'^2 - \rho_2'^2\right)}{2z}\right] J_l\left[\frac{k\,\rho\,\rho_1'}{z}\right] I_{l+m}\left[\frac{\rho_1'\,\rho_2'}{\sigma^2}\right] \times \exp\left[-(\rho_1'^2 + \rho_2'^2)\left(\frac{1}{w^2} + \frac{1}{2\sigma^2}\right)\right] d\rho_1'\,d\rho_2'. \tag{13}$$

The stationary-phase (Sp) approach represents a generally applicable expression suitable for the analysis of axicons. We can defined the SP approximation as

$$I_{\rho'} = \int_A g(\rho')\exp\left[i\,k\,f(\rho')\right] dx, \tag{14}$$

where A denotes aperture area. The slowly varying of the part $g(\rho')$ of the integral is the strength of the incident field or the amplitude variation of an optical element in the aperture. The rapidly varying part $\exp\left[i\,k\,f(\rho')\right]$ contains. From Eq. (13), the total phase of the diffraction formula can be obtained as [19]

$$f(\rho') = (n-1)\,\alpha\,\rho' - \frac{\rho'^2}{2\,z}. \tag{15}$$

The stationary phase obtain as $f'(\rho') = 0$. So in both integration, these stationary points ρ_{Sp}' can be obtained as

$$\rho_{Sp}' = (n-1)\,\alpha\,z, \tag{16}$$

and $f''(\rho') = \frac{1}{z}$ the solution formula can written as

$$I_{\rho'} = g_0 \exp\left[\frac{\pm i\,\pi}{4}\right] \exp\left[i\,k\,f_0(\rho_{Sp}')\right] \sqrt{\frac{2\,\pi}{k\mid f''\,(\rho_{Sp}')\mid}}. \tag{17}$$

The CSD can be obtain as $W_{out}(\rho,z) = \left\langle I_{\rho_1}^* * I_{\rho_2} \right\rangle$. Substituting Eq. (16) into Eq. (13), the numerical formula for the CSD of the PCGSMV beam propagating through the axicon takes the following form

$$W_{out}(\rho,z) = \left(\frac{2\,\pi\,k}{z}\right) G_0(((n-1)\,\alpha)\,z)^2 \times \exp\left[-(((n-1)\,\alpha)\,z)^2\left(\frac{2}{w^2} + \frac{1}{\sigma^2}\right)\right] \times \sum_{-\infty}^{\infty} I_{l+m}\left[\frac{(z\,((n-1)\,\alpha))^2}{\sigma^2}\right] \times J_l\left[k\,\rho\,((n-1)\,\alpha)\right]^2. \tag{18}$$

3. DEPTH OF FOCUS

In axicon, the DOF is expressed as [40, 41]

$$DOF = \frac{w}{(n-1)\,\alpha}. \tag{19}$$

Suppose that the PCGSMV beams exhibit an effective beam width w_{eff} [41, 42], which can be expressed as follows

$$w_{eff} = \left[\frac{1}{(2w)^4} + \frac{1}{(2w)^2\sigma^2}\right]^{-\frac{1}{4}}. \tag{20}$$

Replacing w_{eff} with w in Eq. (19), the DOF of the PCGSMV beam can be expressed as [19, 41]

$$DOF = \frac{\left[\frac{1}{(2w)^4} + \frac{1}{(2w)^2\sigma^2}\right]^{-\frac{1}{4}}}{(n-1)\,\alpha}. \tag{21}$$

4. RESULT AND DISSECTION

Numerical calculations were performed using Mathematica 10. This study was conducted in a Bessel zone, as shown in Fig.1. Based on Eq. (18), the parameters of the PCGSMV beam and classical axicon in the numerical calculation were λ = 632.8 nm, n = 1.7, and G_0 = 1 $watt/mm^2$. Figure 2 shows a comparative analysis of the axial intensity between the (A) PCGSMV and (B) PCGSM beams focused by the classical axicon. The intensity increases with the propagation distance z until it reaches its peak, followed by a gradual decline. In the context of Fig. 2 (A), the effect of the spatial correlation of the coherence length σ on the intensity was elucidated. Notably, the decreases on the intensity with σ, attributed to the vortex effects. Conversely, in Fig. 2 (B), the intensity increases with σ owing to the minimal energy losses as σ increases. Furthermore, there is a discernible shift in the position of the maximum intensity towards large z values in Fig. 2 (A) and (B). The disparity between the outcomes in (A) and (B) is ascribed to the influence of vortex effects. Figure 3 shows the normalized intensity distribution profiles of the PCGSMV beam for different propagation distances and spatial degrees of coherence. As shown in Fig. 3, the beam profile underwent a transition from a half-dark profile to a Gaussian form as it propagates when $\sigma = 2$ mm. Furthermore, there was a concurrent increase in the spot size diameter with propagation. In addition, by increasing the coherence, a dark hollow form with malti-rings, that is, high-order Bessel that transforms into a half-dark profile, then a Gaussian. From Fig. 3, one can see that the distance between the Bessel rings clearly increases the coherence and decreases the propagation owing to the degradation caused by the spatial correlation. High values of σ protected the Bessel form from degradation over a long distance. Our results indicate that a high-order Bessel beam can be generated in a specific ring from PCGSMV using an axicon. The contour plot depicted in Fig. 4 delineates the normalized radial intensity distribution of the PCGSMV beam focused by the axicon as a function of z for various values of σ. As shown in Fig. 4 (A), the vortex effects diminished at a low σ value (specifically, $\sigma = 2$ mm). As shown in Fig. 4 (B), the transformation of the dark hollow shape into a flat-topped shape, which ultimately develops into a Gaussian profile during propagation, is attributed to the degradation of the beam. In Fig. 4 (C), a noticeable reduction in the depth of the dark hollow is observed with propagation. Moreover, a clear appearance of the Bessel rings was evident. Figure 4 (D) illustrates that the beam profile remains conserved along the Bessel zone, particularly at elevated values of σ indicating the role of coherence in mitigating beam degradation. Figure 5 illustrates the radial intensity distribution of the PCGSMV beam shaped by an axicon for various topological charges m. For a PCGSMV beam, it

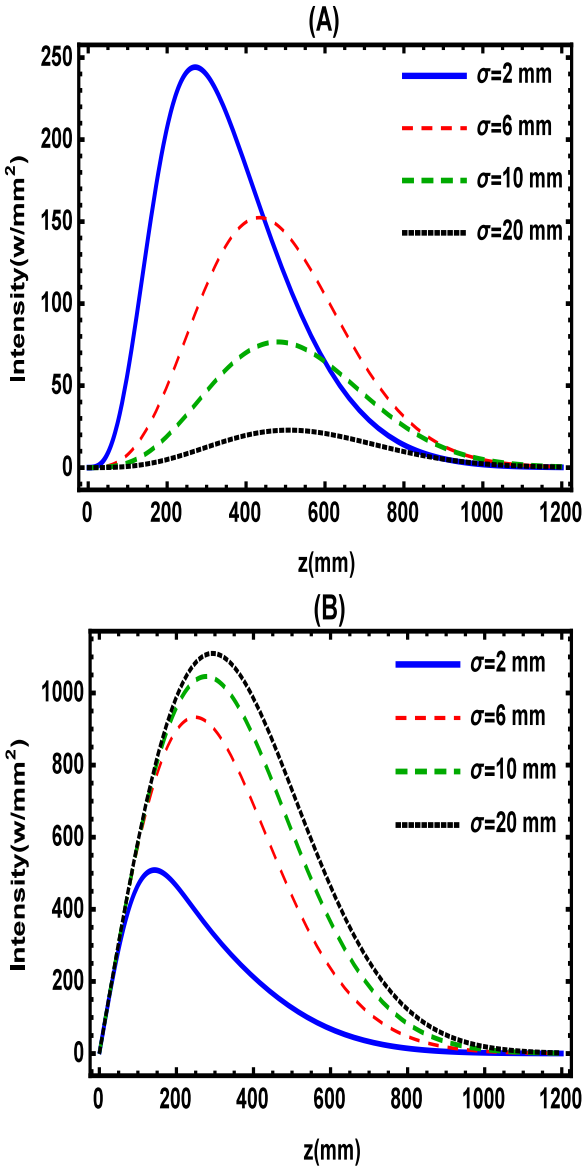

Figure 2. Axial intensity distribution of the (A) PCGSMV beam and (B) PCGSM beam focused by axicon with base angle $\alpha = 0.02$ rad for different values of σ, and $w = 6$ mm.

exhibits a dark hollow beam profile in the source plane. However, its beam profile changes during propagation owing to degradation caused by the spatial coherence of the source. The spot of a partially coherent vortex beam in the focal plane can be manipulated by adjusting the initial coherence width. For instance, the beam profile of the focused beam spot gradually transitions from a dark hollow profile to a flat-topped profile and ultimately to a Gaussian profile as the spatial degree of coherence gradually decreases. Moreover, if the initial coherence width remains constant, it is possible to manipulate the beam spot of a partially coherent vortex beam by changing its initial topological charge [37]. This is because the topological charge acts as a counteracting factor against the degradation caused by coherence. For example, when $\sigma = 2$ mm, the Gaussian beam a transitions to a flat-topped profile and eventually to a dark hollow profile

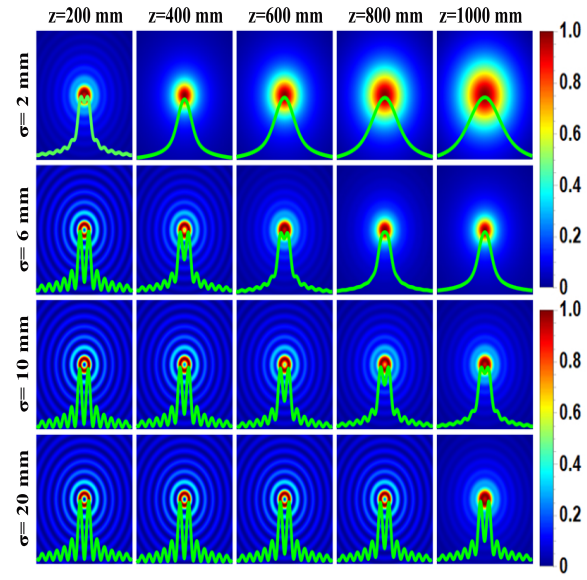

Figure 3. Normalized intensity distribution of the PCGSMV formed by axicon with different propagation distance z and σ for $w = 6$ mm, $m = 1$ and $\alpha = 0.02$ rad.

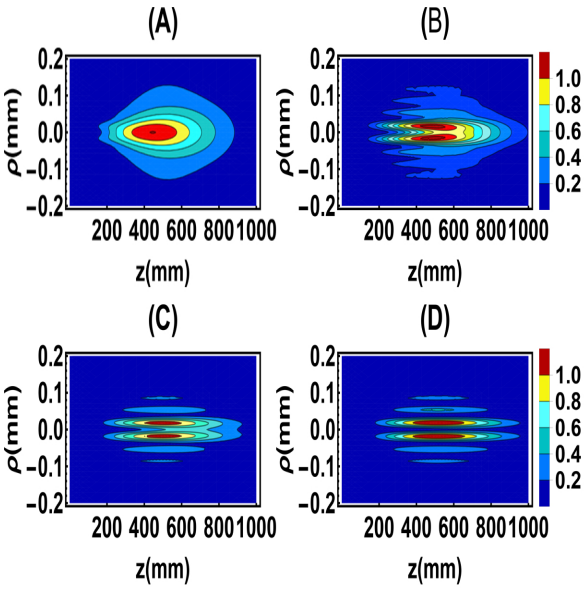

Figure 4. The contour plots of the normalized radial intensity as a function of z for different $\sigma = 2$ mm (A), $\sigma = 6$ mm (B), $\sigma = 10$ mm (C), and $\sigma = 20$ mm (D), $m = 1$, $w = 6$ mm, and $\alpha = 0.02$ rad.

as m increases. The diameter of the diameter dark spot size of the beam increases with topological charge.

Figure 6 depicts the influence of the beam width on the intensity distribution of the PCGSMV beam diffracted by an axicon. It can be observed that the intensity increases with beam width owing to the higher energy carried by the beam width. Additionally, it can be observed that the intensity profile is affected by the propagation owing to the degradation caused by the propagation. The beam spot size gradually transforms from half dark hollow to flat-topped, and eventually into a Gaussian spot size as the propagation distance increases. This transformation was attributed to the degradation of the beam with propagation. Figure 7 (A) shows the effect of the axicon base angle on the intensity distribution at different propagation distances. The curves within this illustration decrease in intensity with the propagation distance. Furthermore, the intensity increases with an increase in α until it reaches its peak. Subsequently, it gradually decreased. Geometrically, the decline in intensity after reaching the maximum value can be attributed to the internal reflection by the axicon. Figure 7 (B) shows the intensity of the PCGSMV beam diffracted by the axicon for different values of σ as a function of the axicon base angle. It was noted that the intensity gradually decreased with an increase in σ owing to the influence of the vortex. This indicated the emergence of a dark spot in the vortex. Furthermore, analysis of Fig. 7 (A) reveals a significant shift in the peak intensity corresponding to an increase in the propagation distance z in the direction of a small α. However, in Fig. 7 (B), the peak intensity shifts with an increase in σ in the direction of increasing α. The 3D intensity distribution of the PCGSMV beam focused by the axicon for the spatial degree of coherence and beam width at $z = 200$ mm and $z = 600$ mm, is illustrated in Fig. 8. It can be observed that the intensity gradual decline with σ attributed to the influence of the vortex. Moreover, an increase in intensity was noticeable as the width of the beam increased. Furthermore, it is observed that the intensity exhibits a linear increase at smaller values of w as w increased. However, for larger values, the relationship becomes non-linear with w. Upon surpassing the diameter of the lens, a fraction of the beam deviates from the axicon, elucidating the constancy in intensity with an increase in the w. Figure 9 (A) depicts the DOF of the PCGSMV beam focused by the axicon as a function of the beam width. It was discovered that the influence of σ on the beam width causes these variations in the curve. Furthermore, the DOF increases quickly for low w values, but slowly as w increases. Figure 9 (B) depicts the change in DOF as a function of σ for various w values. It can be seen that for small σ values, the DOF increases quickly as σ increases; however, for high coherence values, the DOF increases slowly. It can be observed from Fig. 9 that the DOF was 486 mm when $\sigma = 2$ mm, $w = 6$ mm, and $\alpha = 0.02$ rad.

5. CONCLUSION

In this study, a mathematical model was developed based on the PCGSMV beam formula, extended Huygens-Fresnel integral, and the stationary phase method. This model describes the intensity distribution of PCGSMV beam propagation through a classical axicon. Our numerical results demonstrated the effects of the spatial correlation of coherence, beam width, topological charge, and axicon base angle on both intensity distribution and

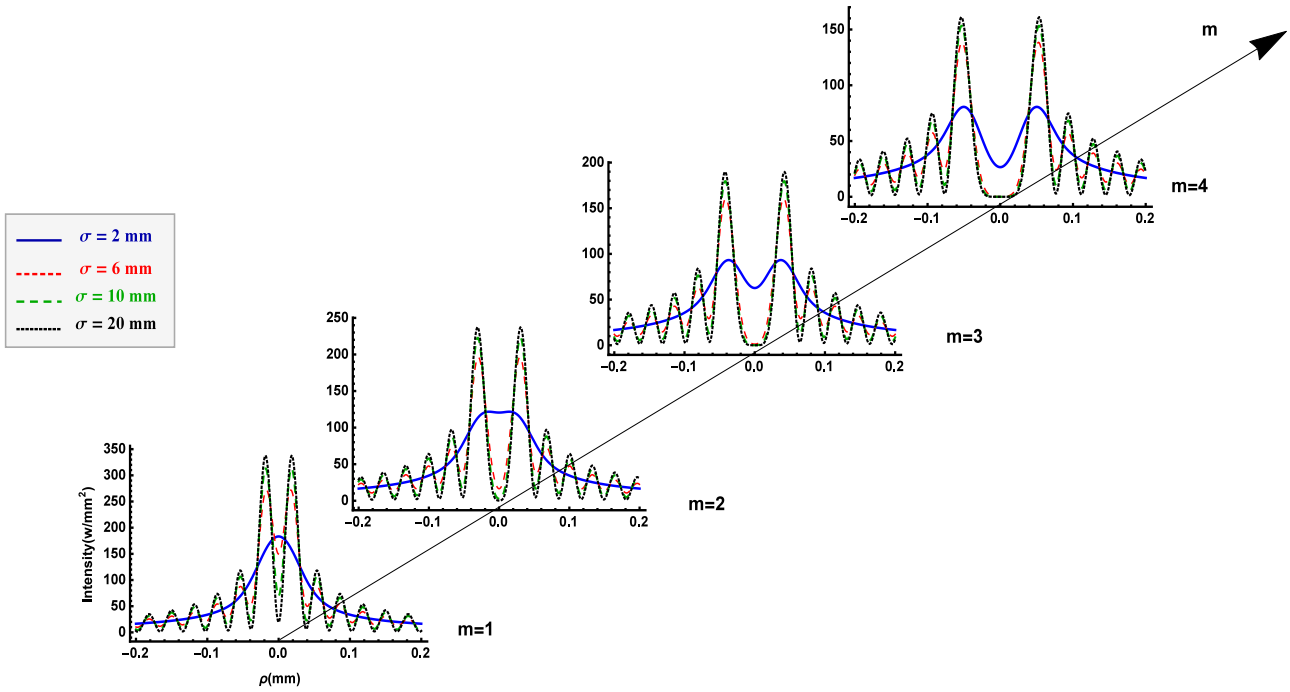

Figure 5. Radial intensity distribution of the PCGSMV beam focused by axicon with base angle $\alpha = 0.02$ rad for several topological charge and several values of σ at $z = 400$ mm and beam width $w = 6$ mm.

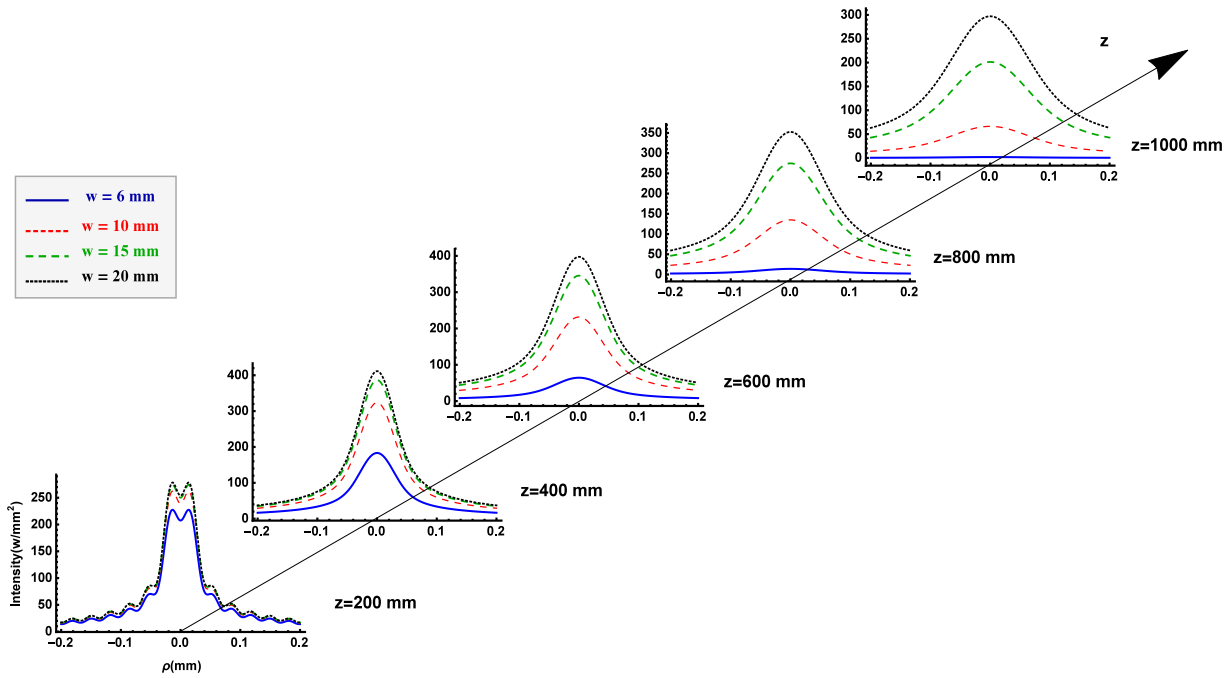

Figure 6. Radial intensity distribution of the PCGSMV beam generated by axicon with base angle $\alpha = 0.02$ rad, $m = 1$, and $\sigma = 2$ mm for several values of w and z.

depth of focus. Our calculations revealed that the intensity and depth of focus increased as the waist width of the beam increase. Our results show that the topological charge plays a role in the anti-degradation caused by coherence. The observed enhancement in the intensity and depth of focus can be attributed to the augmented energy carried by the beam. Conversely, there is a decrease in intensity with an increasing degree of coherence and

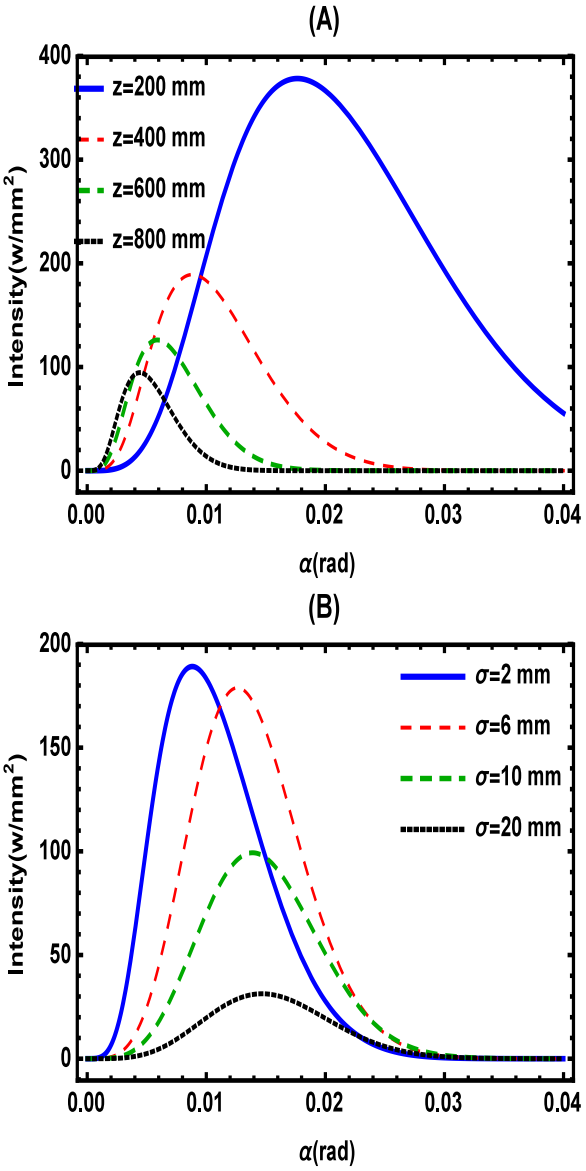

Figure 7. The relation of the intensity distribution of the PCGSMV beam diffracted by classical axicon with axicon base angle (A) at various propagation distance, $\sigma = 2$ mm, and (B) for various spatial correlation of the coherence length, $w = 6$ mm, $m = 1$ and $z = 400$ mm.

topological charge owing to the vortex effect. Our results highlight the intricate interplay between the propagation distance and spectral degree of coherence in the intensity profile. Furthermore, our findings elucidate a notable phenomenon: cancellation of the beam width effect leads to a constant intensity when the beam width aligns with the axicon aperture. We also observed a reduction in DOF with an increase in the axicon base angle. These insights are pivotal for leveraging the diffracted beam by an axicon in various applications, including optical trapping and particle manipulation.

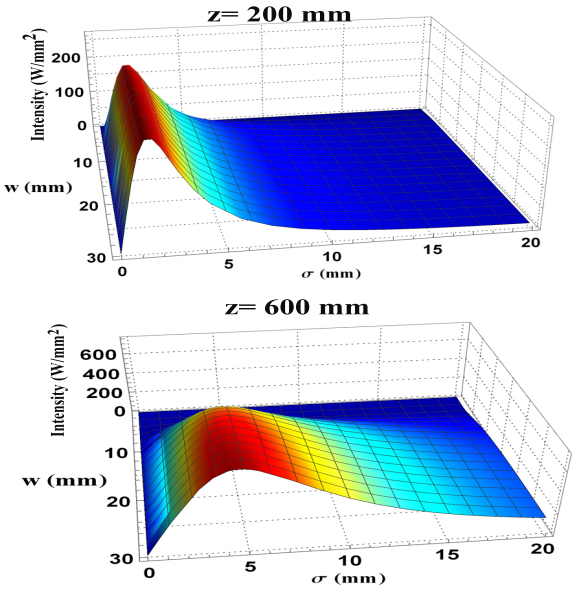

Figure 8. The 3D intensity distribution of the PCGSMV beam focused by axicon with base angle $\alpha = 0.02$ rad and $m = 1$ as a function of beam width and spatial correlation length at $z = 200$ mm and $z = 600$ mm.

REFERENCES

[1] S. N. Khonina, N. L. Kazanskiy, P. A. Khorin, and M. A. Butt, "Modern types of axicons: New functions and applications," Sensors **21**, 6690 (2021).

[2] A. A. Alkelly, H. T. Al-Ahsab, M. Cheng, and I. G. Loqman, "Tight focusing of azimuthally polarized laguerre-gaussian vortex beams by diffractive axicons," Phys. Scr. **99**, 025508 (2024).

[3] M. Shukri, A. A. Alkelly, and Y. S. Alarify, "Apodized design of diffractive axicons for twisted partially coherent light," Appl. Opt. **52**, 1881–1887 (2013).

[4] I. G. Loqman, A. A. Alkelly, and H. T. Al-Ahsab, "Generating double focal spots by focusing a radially polarized double-ring-shaped beam with an annular classical axicon," Opt. Continuum **1**, 1761–1767 (2022).

[5] J. Xia, Z. Yang, H. Chen, *et al.*, "Tangentially and radially polarized nd:yag hollow lasers with two pairs of axicons," Infrared Phys. Technol. **107**, 103301 (2020).

[6] B. K. Gutierrez, J. A. Davis, M. M. Sánchez-López, *et al.*, "Dynamic control of bessel beams through high-phase diffractive axicons," OSA Continuum **3**, 1314–1321 (2020).

[7] S. Saghafi, K. Becker, F. Gori, *et al.*, "Engineering a better light sheet in an axicon-based system using a flattened gaussian beam of low order," J. Biophotonics **15**, e202100342 (2022).

[8] M. Zhang, X. Liu, L. Guo, *et al.*, "Partially coherent flattopped beam generated by an axicon," Appl. Sci. **9**, 1499 (2019).

[9] J.-H. Lin, M.-D. Wei, H.-H. Liang, *et al.*, "Generation of supercontinuum bottle beam using an axicon," Opt. Express **15**, 2940–2946 (2007).

[10] J. H. McLeod, "The axicon: a new type of optical element," J. Opt. Soc. Am.A **44**, 592–10.597 (1954).

[11] M. Rioux, R. Tremblay, and P.-A. Belanger, "Linear, annular, and radial focusing with axicons and applications to laser machining," Appl. Opt. **11**, 1532–1536 (1978).

[12] E. Wright, J. Arlt, and K. Dholakia, "Toroidal optical dipole traps for atomic bose-einstein condensates using laguerre-gaussian beams," Phys.Rev. A **63**, 013608 (2000).

[13] W. Zhang, Y. Lin, Y. Gao, *et al.*, "Numerical and experimental investigation on the optical manipulation from an axicon lensed fiber," Micromachines **12**, 187 (2021).

[14] X. Wang, L. Wang, and S. Zhao, "Propagation properties of an off-axis hollow gaussian-schell model vortex beam in anisotropic oceanic turbulence," J. Mar. Sci. Eng. **9**, 1139 (2021).

[15] A. Beléndez, L. Carretero, and A. Fimia, "The use of partially coherent light to reduce the efficiency of silver halide noise gratings," Opt. Commun. **98**, 236–240 (1993).

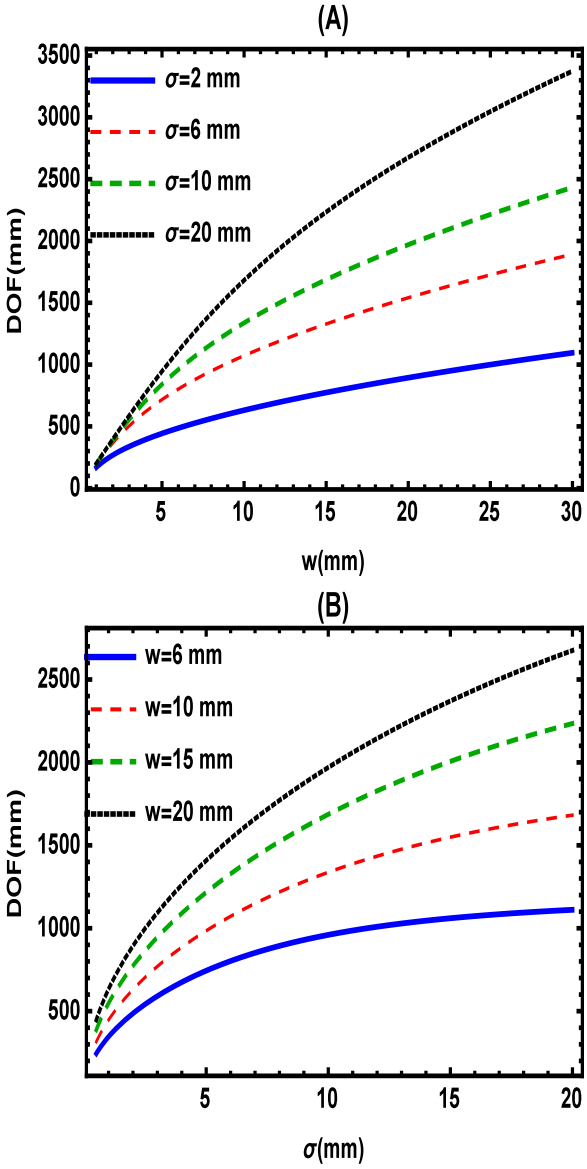

Figure 9. (A) Relation the DOF with w and (B) relation DOF with spatial correlation lengthσ, $\alpha = 0.02$ rad. All curves obtained by the Eq. (21)

[16] Y. Kato, K. Mima, N. Miyanaga, *et al.*, "Random phasing of high-power lasers for uniform target acceleration and plasma-instability suppression," Phys. Rev. Lett. **53**, 1057–1060 (1984).

[17] C. Li, T. Wang, J. Pu, *et al.*, "Ghost imaging with partially coherent light radiation through turbulent atmosphere," Appl. Phys. B **99**, 599–604 (2010).

[18] A. Bhattacharjee, R. Sahu, and A. K. Jha, "Generation of a gaussian schellmodel field as a mixture of its coherent modes," J. Opt. **21**, 105601 (2019).

[19] A. A. Alkelly, M. Shukri, and Y. Alarify, "Intensity distribution and focal depth of axicon illuminated by gaussian schell-model beam," Opt. Commun. **284**, 4658–4662 (2011).

[20] C. Zhao, Y. Cai, X. Lu, and H. T. Eyyuboglu, "Radiation force of coherent and partially coherent flat-topped beams on a rayleigh particle," Opt. Express **17**, 1753–1765 (2009).

[21] Y. Lu, C. M. Holland, and L. W. Cheuk, "Molecular laser cooling in a dynamically tunable repulsive optical trap," Phys. Rev. Lett. **128**, 213201 (2022).

[22] C. Zhao and Y. Cai, "Trapping two types of particles using a focused partially coherent elegant laguerre–gaussian beam," Opt. Lett. **36**, 2251–2253 (2011).

[23] S. N. Khonina and S. A. Degtyarev, "Analysis of the formation of a longitudinally polarized optical needle by a lens and axicon under tightly focused conditions," J. Opt. Technol. **83**, 197–205 (2016).

[24] J. Xu, T. Geng, X. Gao, and S. Zhuang, "Generation of a dark spot beyond the diffraction limit with a radially polarized vortex beam," J. Opt. Soc. Am.A **34**, 2165–2169 (2017).

[25] J. Zeng, R. Lin, X. Liu, *et al.*, "Review on partially coherent vortex beams," Front. Optoelectron. **12**, 229–248 (2019).

[26] A. AlKelly, I. G. Loqman, and H. T. Al-Ahsab, "Focus shaping of cylindrically polarized vortex beams by a linear axicon," Electron. J. Univ. Aden for Basic Appl. Sci. **2**, 145–150 (2021).

[27] M. S. Qusailah, A. A. Alkelly, W. A. Al-Bahry *et al.*, "The propagation properties of a lorentz–gauss vortex beam in a gradient-index medium," Int. J. Opt. **2023** (2023).

[28] A. A. Alkelly, M. Khaled, and L. F. Hassan, "Angular width and beam quality of a partially coherent standard laguerre–gaussian vortex beam in turbulent plasma," JOSA A **41**, 45–53 (2024).

[29] H. AL-Nadary, A. A. Alkelly, M. Khaled, and L. F. Hassan, "The effective beam width of a partially coherent rectangular multi-gaussian schell-model vortex beam propagating in a turbulent plasma," Sana'a Univ. J.of Appl. Sci. Technol. **1** (2023).

[30] S. Chang, Y. Song, Y. Dong, and K. Dong, "Spreading properties of a multigaussian schell-model vortex beam in slanted atmospheric turbulence," Opt. Appl. **50** (2020).

[31] X. Ma, G. Wang, H. Zhong, *et al.*, "The off-axis multigaussian schell-model hollow vortex beams propagation in free space and turbulent ocean," Optik **228**, 166180 (2021).

[32] Y. Pan, M. Zhao, M. Zhang, *et al.*, "Propagation properties of rotationally-symmetric power-exponent-phase vortex beam through oceanic turbulence," Opt. Laser Technol. **159**, 109024 (2023).

[33] M. Duan, Y. Tian, and J. Li, "Propagation of gaussian schell-model vortex beams in biological tissues," Opt. Appl. **49**, 203–215 (2019).

[34] A. A. Alkelly, M. Khaled, and L. F. Hassan, "Influence of anisotropic turbulent plasma on the partially coherent four-petal gaussian vortex beams," Electron. J. Univ. Aden for Basic Appl. Sci. **3**, 145–151 (2022).

[35] A. A. Alkelly, M. Khaled, and L. F. Hassan, "Spreading properties of partially coherent multi-gaussian schell-model and modified bessel-correlated vortex beams in anisotropic turbulent plasma," Phys. Scripta **98**, 075518 (2023).

[36] R. Lian-Zhou and P. Ji-Xiong, "Focusing of partially coherent vortex beams by an aperture lens," Chin. Phys. Lett. **24**, 1252 (2007).

[37] X. Liu, L. Liu, Y. Chen, and Y. Cai, "Partially coherent vortex beam: from theory to experiment," Vortex Dyn. Opt. Vortices pp. 275–296 (2017).

[38] M. Born and E. Wolf, *Principles of optics: electromagnetic theory of propagation, interference and diffraction of light* (Elsevier, 2013).

[39] I. S. Chowdhury, R. P. Roberts, G. Molina-Terriza, and X. Vidal, "Lensaxicon separation to tailor aberration free focused bessel-gaussian beams in the paraxial regime," Opt. Express **27**, 11160–11173 (2019).

[40] S. N. Khonina, N. L. Kazanskiy, S. V. Karpeev, and M. A. Butt, "Bessel beam: Significance and applications—a progressive review," Micromachines **11**, 997 (2020).

[41] M. S. Qusailah, A. A. Alkelly, H. Al-Nadary, *et al.*, "Depth of focus and intensity distribution of a lensacon illuminated by a partially coherent gaussian schell vortex beam," Appl. Opt. **63**, 3138–3147 (2024).

[42] M. A. Shukri, A. A. Alkelly, and Y. S. Alarify, "Spatial correlation properties of twisted partially coherent light focused by diffractive axicons," J. Opt. Soc. Am.A **29**, 2019–2027 (2012).